Scalable, solvent-free transparent film-based air filter with high particulate matter 2.5 filtration efficiency

Woo Jin Lee [a,b,1], Seungtae Oh [a,1], Jong-Eun Park [c], Jungho Hwang [b,*], Hyeonjin Eom [a,*]

[a] Carbon Neutral Technology R&D Department, Korea Institute of Industrial Technology, Cheonan 31056, Republic of Korea
[b] Department of Mechanical Engineering, Yonsei University, Seoul 03722, Republic of Korea
[c] Department of Mechanical Engineering, The State University of New York Korea, Incheon 21985, Republic of Korea

HIGHLIGHTS

- Transparent film-based air filter with high filtration efficiency is developed.
- Corona discharging and punch stamping are strategically employed.
- Suggested fabrication method is microplastic-free and solvent-free.
- Film-based filter retains 99.9 % particulate matter 2.5 filtration efficiency.
- Transparency of film-based filter enables clear visibility of facial expressions.

GRAPHICAL ABSTRACT
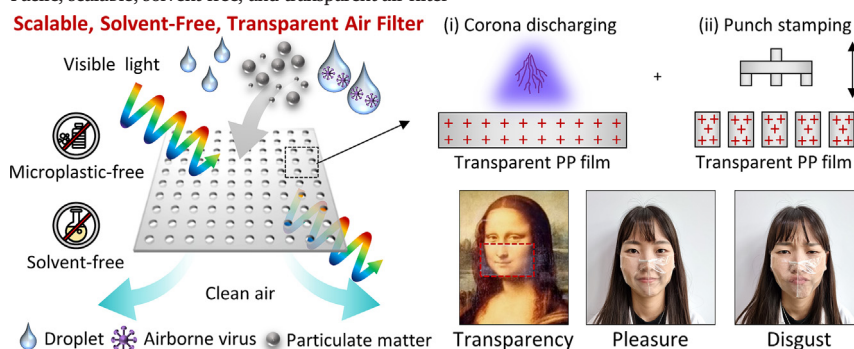
ARTICLE INFO

Editor: Pavlos Kassomenos

ABSTRACT

Over the course of the COVID-19 pandemic, people have realized the importance of wearing a mask. However, conventional nanofiber-based face masks impede communication between people because of their opacity. Moreover, it remains challenging to achieve both high filtration performance and transparency through fibrous mask filters without using harmful solvents. Herein, scalable transparent film-based filters with high transparency and collection efficiency are fabricated in a facile manner by means of corona discharging and punch stamping. Both methods improve the surface potential of the film while the punch stamping procedure generates micropores in the film, which enhances the electrostatic force between the film and particulate matter (PM), thereby improving the collection efficiency of the film. Moreover, the suggested fabrication method involves no nanofibers and harmful solvents, which mitigates the generation of microplastics and potential risks for the human body. The film-based filter provides a high $PM_{2.5}$ collection efficiency of 99.9 % while maintaining a transparency of 52 % at the wavelength of 550 nm. This enables people to distinguish the facial expressions of a person wearing a mask composed of the proposed film-based filter. Moreover, the results of durability experiments indicate that the developed film-based filter is anti-fouling, liquid-resistant, microplastic-free and foldability.

1. Introduction

Since the outbreak of the COVID-19 pandemic, our lives have substantially changed. COVID-19 is readily spread through viruses and droplets floating in the air. Moreover, particulate matter (PM), which is generated by environmental pollution and floats in the air, enters the body during

* Corresponding authors.
  E-mail addresses: hwangjh@yonsei.ac.kr (J. Hwang), hyeonjin@kitech.re.kr (H. Eom).
  [1] These authors contributed equally.

the respiration process and causes diseases such as respiratory diseases, cardiovascular diseases, strokes, and even cancer (Brugge et al., 2017; Chen et al., 2019; Gong et al., 2014; Lane et al., 2016; Martinelli et al., 2013). One of the most promising strategies for preventing COVID-19 infection and PM inhalation is wearing a face mask, as reported by the World Health Organization (WHO) (Howard et al., 2021; Rader et al., 2021; Shekaraiah and Suresh, 2021; Ueki et al., 2020; World Health Organization, 2020), because it prevents infection by blocking harmful substances such as droplets, viruses, COVID-19, and PM.

Many studies have reported composite air filters with improved filtration performance (Bian et al., 2020; Desai et al., 2009; Lavoie et al., 2020; Liu et al., 2020; Wang et al., 2016b; Yang et al., 2019; Zhang et al., 2018). These filters are composed of fiber materials such as polypropylene (PP), polyacrylonitrile (PAN), polysulfonamide (PSA), polyethylene terephthalate (PET), and polyurethane (PU) (Table 1). Among them, many filters employ PP nanofibers and are prepared using melt-blowing (MB) methods that generate nanofibers from an extruder at high temperatures (Lavoie et al., 2020; Zhang et al., 2018). These filters exhibit a high filtration performance of 99.2 % and low pressure drop of 92 Pa (Zhang et al., 2018). A filter prepared from PAN and PSA exhibited a high $PM_{2.5}$ collection efficiency of 99.52 % and was thermally stable at 300 °C (Yang et al., 2019). Several researchers have investigated eco-friendly filters comprising natural materials such as silk (Wang et al., 2016b) and chitosan (Desai et al., 2009). The silk-based composite filter was reported to be biologically compatible and light weight at 3.4 g/m^2 (Wang et al., 2016b).

Although these approaches provide enhanced filtration performance, they limit communication in interpersonal relationships owing to their opacity (Marler and Ditton, 2021; Miyazaki et al., 2022). People interpret other people's emotions from their facial expressions (Ioannou et al., 2005). Especially, the lower half of the face is an important area for interpreting their emotions. For example, the mouth of a person plays an essential role in expressing emotions, and other parts of the face such as dimples and facial muscles contribute to emotional expression (Carbon, 2020; Gori et al., 2021; Grenville and Dwyer, 2022; Kim et al., 2022; Nestor et al., 2020). However, when a person wears a mask, the lower part of their face is obscured, which limits other people from understanding their emotions. In particular, children are adversely affected by such communication because they require natural interaction with other people (Gori et al., 2021). Therefore, the demand for a transparent mask for people who need such visual assistance in interpersonal communication has increased rapidly.

Many researchers have attempted to develop transparent filters by using electrospun nanofibers (Cui et al., 2021; Liang et al., 2019; Liu et al., 2015,

2019; Mikheev et al., 2016; Wang et al., 2020; Xu et al., 2016; Zhao et al., 2016) (Table 1). For example, Liu et al. reported PDMS/PMMA-chitosan filter exhibited a high PM collection efficiency exceeding 96 % owing to the small diameter of the fibers and polar chemical functional groups, while it retained a high transmittance of 86 % (Liu et al., 2019). Liang et al. reported a thermoplastic polyurethane (TPU)-based filter with $PM_{2.5}$ collection efficiency of 99.6 % and optical transmittance of 60 % by electrospinning TPU onto a conductive mesh (Liang et al., 2019). A few researchers have investigated transparent filters prepared by electrospinning high-dipole-moment materials such as polyacrylonitrile (PAN) and nylon-6 on a mesh (Liu et al., 2015; Xu et al., 2016). PAN-based filters with high dipole moments exhibit $PM_{2.5}$ collection efficiencies exceeding 95 % and transmittance levels exceeding 90 % (Liu et al., 2015). Other researchers have suggested the use of modified electrospinning techniques in conjunction with electrostatic spraying (Mikheev et al., 2016) or bipolar electrospinning (Wang et al., 2020) to prepare filters. For example, polymer filters manufactured using the bipolar electrospinning method exhibit $PM_{2.5}$ collection efficiencies exceeding 98 % and transmittance levels exceeding 70 % (Wang et al., 2020). However, all these aforementioned strategies for fabricating transparent masks have limitations due to their use of harmful solvents or additives such as formic acid and *N, N*-dimethylformamide (DMF). These pose risks to human health and the environment and complicate filter manufacturing (Lv et al., 2018). Although Cui et al. investigated a PVA filter fabricated using water, its filtration performance decreased in humid environments (Cui et al., 2021). In addition, electrospun nanofibers are difficult to use independently as a mask owing to their poor mechanical characteristics (Grafe and Gragam, 2003), which inevitably encourages their incorporation with support materials such as metal meshes and fabrics. Furthermore, the recycling of composite filters is hampered by fibers, thermoset matrices, and binders from composite materials (Yang et al., 2012). More importantly, many studies have reported that many microplastics originate from fibers (Acharya et al., 2021; Aragaw, 2020; Dris et al., 2016; Morgana et al., 2021; Shen et al., 2021; Shruti et al., 2021; Zhang et al., 2020). This exposes mask wearers to microplastics, which can pose to human risks such as oxidative stress and neurotoxicity (Matthews et al., 2021; Prata et al., 2020; Rai et al., 2021).

To address these issues, in this study, we develop a facile, scalable, and solvent-free film-based approach to fabricate filters composed of transparent polypropylene (PP) films that can be applied as face masks by themselves. The proposed filters are fabricated using the corona discharge and facile stamping processes. This synergetic fabrication strategy increases the surface potential of the filters relative to that of the PP film surface, thus leading to enhanced attraction between filters and PM. The film-

Table 1
Previously reported opaque and transparent filters.

Transparency	Ref.	Material	Solvent or additive	Fabrication method	Filter type
Opaque	Lavoie et al., 2020	PP	Fluorochemical melt additive	Melt-blowing	Fiber
	Zhang et al., 2018	PP	MgSt[a]	Melt-blowing	Fiber
	Yang et al., 2019	PAN, PSA	DMAc[b]	Electrospinning	Fiber on fabric or SUS mesh
	Liu et al., 2020	PET, PU	DMF[c]	Electrospinning	Fiber on micro-fibrous PET
	Wang et al., 2016b	Silk	Acetic acid	Electrospinning	Fiber on silk chiffon
	Desai et al., 2009	Chitosan, PEO	Formic acid	Electrospinning	Fiber on spunbonded PP
	Bian et al., 2020	Nylon	Formic acid	Electrospinning	Fiber on Cu mesh
Transparent	Liu et al., 2019	PMMA, PDMS, Chitosan	DMF[c]	Electrospinning	Fiber on wire mesh
	Zhao et al., 2016	PAN	DMF[c]	Electrospinning	Fiber
	Liang et al., 2019	TPU	DMF[c]	Electrospinning	Fiber on conductive mesh
	Liu et al., 2015	PAN	DMF[c]	Electrospinning	Fiber on a fiberglass wire mesh
	Xu et al., 2016	Nylon-6	Formic acid	Electrospinning	Fiber on metallic foil
	Mikheev et al., 2016	Nylon-4,6	Formic acid	Electrospinning and Electrospraying	Fiber
	Wang et al., 2020	PAN, TPU, PVA, PS	DMF[c], DI water	Electrospinning	Fiber on mesh
	Cui et al., 2021	PVA	DI water, SLS[d], CTAB[e]	Electrospinning	Fiber on fabric
	This work	PP	–	Corona discharging and Punching	Film

[a] Magnesium stearate.
[b] *N,N*-dimethylacetamide.
[c] *N,N*-dimethylformamide.
[d] Sodium lignosulfonate.
[e] Hexadecyl trimethyl ammonium bromide.

based filters prepared herein simultaneously exhibit superior filtration and transparency characteristics, such as a $PM_{2.5}$ collection efficiency of 99.9 % and transmittance of 52 % at 550 nm while maintaining low pressure drops. The theoretical findings obtained from an optical simulation that is performed considering the structural and optical characteristics of these films support their transparency. Moreover, the proposed transparent film-based filters are environmental-friendly and nontoxic because harmful solvents are not used in the manufacturing process. More importantly, PP does not cause skin irritation (Gitsas and Floudas, 2008; Park et al., 2012; Paula E Silva et al., 2001), and the films fabricated herein are microplastic-free. Also, the proposed film-based filters exhibit superior foldability, and durability, making them highly suitable for use as mask. They maintain their initial state after contamination and can be cleaned by following a simple washing process. In addition, they exhibit liquid resistance against hydrostatic pressure and prevent liquid penetration. Furthermore, they leave no residuals on the tape in the tape peeling test, which implies their microplastic-free property during usage as a face mask.

2. Experimental section

2.1. Fabrication of transparent micropore film

Transparent PP films (DF1420-7S, Dreamdepot Korea Ltd.) were treated using a corona discharge reactor (PLASMA & CORONA SYSTEM, System Korea Ltd.). The corona discharge power was set to 0.1–0.8 kW, and a transparent film was fixed onto the reactor plate. The corona-discharged films were placed on PVC pad and punched using a commercial needle array stamp (MTS 80 Derma Stamp, L'arcobaleno Ltd.) to obtain microporous films. The number of micropores was controlled by adjusting the number of punch stamping runs. The prepared samples were named depending on the process by which they were fabricated, as follows: the letters represent the fabrication process, that is, C: corona-discharged, PC: punch-stamped and corona discharged, and CP: corona-discharged and punch-stamped, while the number indicates the micropore density, that is, the number of pores per unit filter area ($\#/cm^2$) (e.g., 75, 150, 300, and 1052). For example, CP1052 denotes a sample fabricated using corona discharging and punch stamping processes in that order, and it has 1052 pores per unit area.

2.2. Evaluation of structural and electrostatic characteristics

Surface images of the microporous films fabricated herein were captured using a laser confocal microscopy (VK-X200, KEYENCE Ltd.). The average micropore diameter and packing density of the films (i.e., solid volume/total volume) were calculated using Image J software (Image J 1.49v, National Institutes of Health).

The surface potentials of the sample were measured using an electrostatic voltmeter (Model 542A, Trek Inc.). The distance between the sample and measurement terminal was maintained at 1 cm. Five measurements were conducted for each film, and the average of the measured values was computed. The surface charge densities of the filters were calculated using Eq. (1), as follows (Reedyk and Perlman, 1968; Yovcheva et al., 2007).

$$(\sigma - P_s) = \frac{\varepsilon_r \varepsilon_0 V_B}{d} \tag{1}$$

where $(\sigma - P_s)$, ε_0, and ε_r denote the net surface charge density (C/m^2), permittivity of vacuum ($\varepsilon_0 = 8.854 \times 10^{-12}$ F/m), and dielectric constant of PP film at 1 kHz ($\varepsilon_r = 2.27$) (Yuan and Chung, 2011), respectively; V_B is the surface potential (kV); and d is the sample thickness (70 μm). The sample thickness was measured using a constant-pressure thickness gauge (FFD-1, Peacock). The dielectric constant, thickness, surface potential, and calculated surface charge density are summarized in Table S1.

2.3. Evaluation of filtration performances

The filtration performances of the transparent microporous film and commercial melt-blown filter (MB filter) were evaluated. The filtration characteristics of commercially available MB filters (denoted as MB1, MB2, and MB3) were compared to those of the proposed microporous film filters. Information pertaining to the manufacturers of these commercially available filters was not included to prevent any controversy.

The pressure drops of the filters were measured using a manometer (510, Testo Inc.) at the filtration velocities of 1–15 cm/s. The filters were placed in a stainless-steel filter holder (2220, Pall Inc.), and the differences between their upstream and downstream pressures were measured to quantify their pressure drops; the filtration velocities were adjusted using a vacuum pump (DOA-P704-AC, GAST Ltd.). The collection efficiencies of the proposed filters were measured using an aerodynamic particle sizer (APS; 3321, TSI Inc.) in the filtration velocity range of 1–15 cm/s. The injected Arizona test dust (ATD A1, PTI Inc.) was passed through a filter holder housing a filter, and the collection efficiencies of the filters were evaluated by comparing the number of concentrations at the inlet and outlet of the APS. The collection efficiencies (E) of the filters were calculated using Eq. (2), as follows (Ahn et al., 2022; Wang et al., 2016a).

$$E = 1 - C_o/C_i \tag{2}$$

where C_i and C_o denote the number particle concentrations at the inlet and outlet of the APS, respectively.

A permeability test of water vapor for comfortable respiration was conducted using custom-built apparatus as shown in Fig. S1a. Thermohygrometer was placed at the outlet, where water vapor from the steam generator passed through the sample. During the test, the relative humidity was measured over time.

2.4. Transmittance measurement

The transmittance of the prepared films was measured using a UV–vis spectrometer (Lambda 750S, PerkinElmer) in the wavelength range of 250–800 nm. Photo images for transparency validation were captured by using a smartphone (Galaxy S20 Ultra, Samsung Electronics Co.).

2.5. Optical simulation

The finite difference time domain (FDTD) method (Lumerical FDTD Solutions, 2018) was used to investigate the transmittance of the prepared CP film and MB filters. The refractive index of PP was taken as 1.5 (Yovcheva et al., 2008), and a plane wave was used as the light source in the visible wavelength range of 400–700 nm along the Z-axis. The simulations were performed on a square-type periodic micro-hole array structure with a hole diameter and period of 70 and 250 μm, respectively, in the case of the CP films (Fig. S2). A cylindrical hexagonal lattice with a layer-after-layer structure was utilized for the MB filters, and the pore diameter and horizontal period of this structure were 2.8 and 8 μm, respectively. The adjacent layers crossed at a right angle with a distance of 8 μm, resulting in a vertical period of 32 μm. The simulation region was set as each unit area of the periodic structures in the X and Y directions, while the thickness of the CP film and MB filters were fixed at 50 μm and 250 μm, respectively, considering the unit cell size and memory requirements. The mesh size of the CP film was uniformly set at 200 nm, 200 nm, and 5 nm along the X, Y, and Z directions, and an auto non-uniform mesh with a minimum step of 0.25 nm was set for the MB filter. The periodic and perfectly matched layer (PML) boundary condition was applied in the horizontal and vertical directions for both filters, and the power monitor was positioned 10 nm and 30 μm below the CP films and MB filters, respectively.

2.6. Characterization of durability

A liquid resistance test of the samples was conducted using the method prescribed in the "KF-AD Detailed Approval Plan Guide" published by the Ministry of Food and Drug Safety of Korea. After fixing the filter with a

rubber band at the rim of a beaker filled with water, we turned it over and left it for 2 h. A piece of paper was placed under the beaker to inspect for water passage through the filter. In the antifouling test, 3 g of Arizona dust was collected in the filter after several filtration processes. After washing the filter with running water, it was dried at room temperature, and its surface was observed using a laser confocal microscopy. A tape test was performed using scotch tape (3 M Co.) to investigate the surface adhesion of the films, which is related to the introduction of microplastics in users' bodies. In the abrasion test, prepared samples were abraded with #400 mesh sandpaper, while the constant pressure of 511 Pa (90.2 g weight/ 17.3 cm^2 area) was applied onto the sample with the abrasion length of 10 cm (Oh et al., 2022b, 2019; Shim et al., 2023).

3. Results and discussion

3.1. Fabrication of transparent microporous film

Fig. 1a schematically illustrates the proposed film-based filter that can block pollutants such as PMs and droplets, including viruses, while transmitting light. To realize the transparent film-based filter, we employed a synergetic fabrication strategy involving corona discharging and stamp punching (Fig. 1b). The rationale underlying this strategy is based on the fact that both corona discharging and stamp punching substantially improve the surface potential of a transparent PP film, while punching results in the formation of micropores on the film. This design strategy is important because a film with high surface potential is more effective for PM collection owing to enhanced electrostatic force (Fig. 1c) (Fatihou et al., 2017). Furthermore, this PM collection mechanism seldom leads to micropore blockage, resulting in sustained air permeation (Fig. 1d). Simultaneously, because the proposed strategy does not employ any harmful solvents or nanofibers such as PAN, PSA, and PET, potential risks for the human body, microplastic generation and incident light scattering can be substantially reduced. The optical characteristics of the proposed microporous film allowed for high transparency of the proposed filter when it was applied to paintings such as the Mona Lisa without any visual degradation (Fig. 1e). When a person wore a face mask composed solely of the proposed filter,

their entire face including the lower half was readily recognizable, which allowed others to understand their facial expressions (Fig. 1f).

To obtain the above-described transparent filter, we first treated a PP film with the corona-discharging process (Fig. 2a). Only the corona-discharged PP film (denoted as "C" film) was roughened (Cáceres et al., 2012; Vassiliadi and Tarantili, 2007) because corona discharging converted C=C stretching into C—O and C=O stretching, resulting in the formation of oxidized groups on the PP film surface (Fig. 2b) (Song et al., 2007; Strobel et al., 2003; Tuominen et al., 2010). This induced the formation of functional groups, cross-linking, chain scission, and breaking of long-chain molecules (Fig. 2a,b) (Song et al., 2007; Strobel et al., 2003; Tuominen et al., 2010). After corona discharging, micropores were generated in the corona-discharged PP film (denoted "CP" film) by subjecting it to punch stamping (Fig. 2b). The pore number densities (*N*) of the films were controlled precisely by varying the number of punch-stamping process runs, and the fabricated films had 75, 150, 300, and 1052 pores/cm^2 (Fig. S3a,b). Thus, punch stamping allows one to adjust the *N* of a filter. Fig. 2c depicts the camera images obtained at each of the fabrication steps illustrated in Fig. 2a. Notably, the fabricated film retains its transparency after corona discharging and punch stamping (Fig. 2c).

Moreover, we observed that the pore size of the fabricated film retained its linearity with respect to *N* (Fig. 2d). This was attributed to the fact that PP is a semicrystalline polymer composed of amorphous and crystalline structures (Lin et al., 2018; Martinez et al., 2022). When it is exposed to a repetitive external stimulus, for example, punch stamping, the amorphous phase of PP remedies the deformed parts in the film (i.e., punched area), which reduces the pore size (Fig. 2d and Fig. S3c) (Lin et al., 2018). In addition, the pore size distribution of the CP film exhibited a Gaussian distribution curve, whereas the pore size of the PC film was randomly distributed owing to the presence of pores measuring >300 μm (Fig. S4). In the case of the PC film, when the punched films were treated with corona discharging, their pore size partially increased up to >300 μm owing to the aforementioned corona discharging effect such as chain scission (Fig. S4 and Fig. S5), which can impede their filtration performances (Fig. S6). Hence, we optimized the fabrication procedure by performing the corona-discharge treatment before punch stamping.
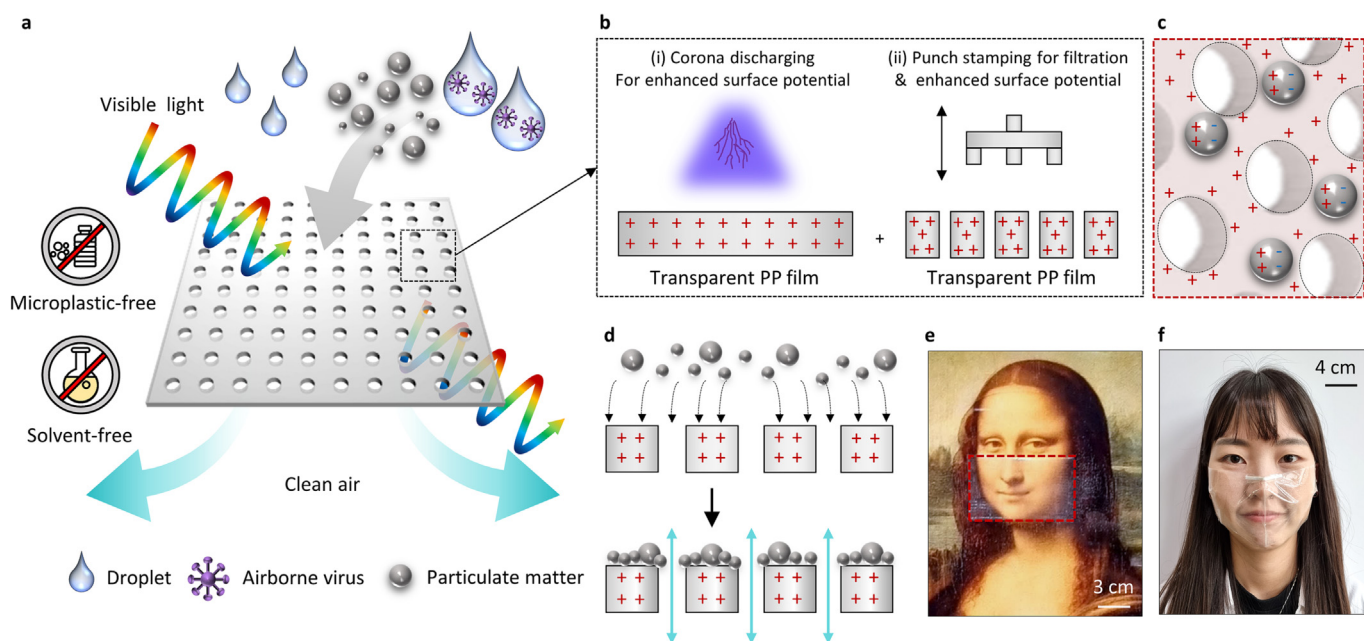

Fig. 1. Facile, scalable, solvent-free, and transparent microporous filter. (a) Schematic illustration of proposed film-based filter. (b) Synergetic fabrication strategy involving corona discharge and stamp punching. (c,d) PM collection and air permeation mechanisms via enhanced electrostatic force of microporous film surface. (e,f) High transparency of microporous film filter; (e) Photographs of microporous film filter on paintings (Scale bar: 3 cm; red dotted line indicates area covered by filter), and (f) Photographs of a person wearing a face mask composed of the proposed microporous film filter (Scale bar: 4 cm).
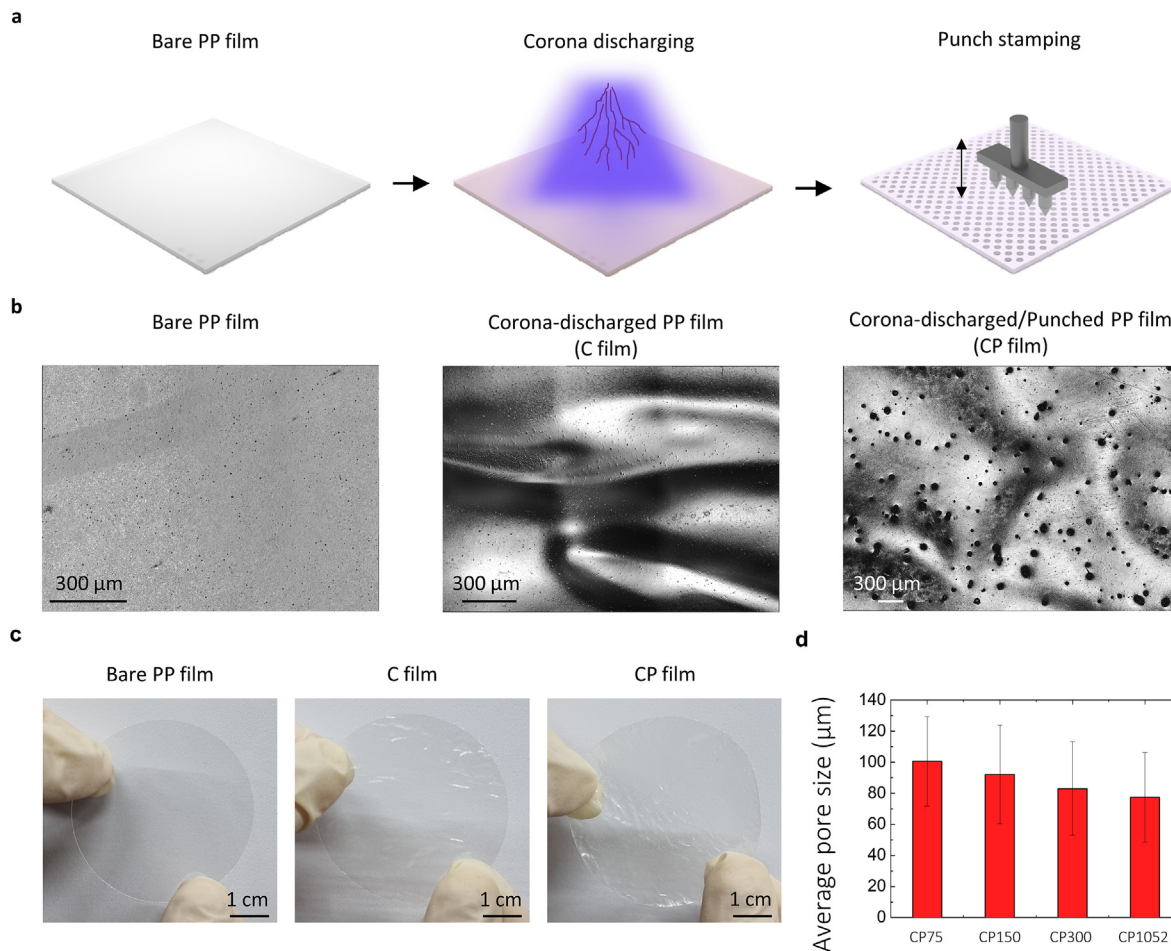
a

Bare PP film   Corona discharging   Punch stamping

b

Bare PP film   Corona-discharged PP film   Corona-discharged/Punched PP film
                              (C film)   (CP film)

c

Bare PP film   C film   CP film

d

Fig. 2. Fabrication of transparent microporous film. (a) Schematics describing steps for fabrication of the microporous film. (b) Laser confocal microscopy images obtained in each fabrication step. Scale bar: 300 μm. (c) Photographs captured in each fabrication step. Scale bar: 1 cm. (d) Average pore size of CP films with different pore number densities.

3.2. Filtration capability

To investigate the viability of the proposed CP films in terms of comfortable respiration, we determined the pressure drop values of the CP film under different filtration velocities (Fig. 3a). Moreover, the punch-stamped films without corona-discharging treatment (denoted "P" film) were investigated for comparison (Fig. S7a). We observed that the CP and P films with N values of 75 and 150 (i.e., CP75, CP150, P75, and P150) retained pressure drop values exceeding 1000 Pa at the filtration velocity of 5.3 cm/s because of their limited pore number densities (Fig. 3a and Fig. S7a). By contrast, the CP300 and CP1052 films retained low pressure drops. Especially, the pressure drop of CP1052 is 87 Pa at a filtration velocity of 15 cm/s, which outperforms other CP films. Therefore, we selected these films for filtration performance evaluation (i.e., CP300 and CP1052).

Fig. 3b shows the collection efficiencies of selected films with respect to the particle diameter of dust. Notably, the collection efficiencies of the tested film filters with an N value of 1052 (i.e., CP1052 and P1052) surpasses those of the films with an N value of 300 (i.e., CP300 and P300) over a range of particle diameters, despite having low packing density (Fig. 3b and Table S2). Moreover, the CP films retain higher levels of collection efficiency than the P films with the same N value. Especially, the CP1052 film exhibits superior collection efficiencies of 99.9 % for PM_{10} and 86.0 % for $PM_{2.5}$, despite having a larger average pore size than the P1052 film (Table S2). To elucidate the improved collection efficiency of the CP film, we compared the PM_{10} collection efficiencies of the tested films with their surface potentials. As shown in Fig. 3c, the surface potential of the C film is 0.27 kV, which represents an improvement of approximately

450 % over the surface potential of 0.06 kV of the untreated bare PP film. Similarly, the surface potentials of the CP films (0.30 kV for CP300 and 0.36 kV for CP1052) are higher than those of the P films with the same N values (0.24 kV for P300 and 0.28 kV for P1052). These results indicate that the corona-discharge treatment substantially enhances the surface potentials of the films. Moreover, the surface potentials of the films with high N values (i.e., CP1052 and P1052) exceed those of the films with low N values (i.e., CP300 and P300). This indicates that the punch-stamping process not only generates circular pores in the films but also increases their surface potential. This enhancement in surface potential increases the surface charge density of the films (Fig. 3c and Table S1) (Reedyk and Perlman, 1968; Yovcheva et al., 2007). The enhanced surface charge density improves the electrostatic force, as expressed in Eqs. (3) and (4). The relationship between the surface charge density of the films and applied electric field is defined in Eq. (3) (Li et al., 2011).

$$E_0 = (4\pi/\varepsilon)\sigma_0 \qquad (3)$$

where E_0, ε, and σ_0 denote the electrostatic field strength at the particle surface (V/dm), dielectric constant, and surface charge density of charged particles (C/dm²), respectively. Moreover, the electric field appears in the relationship with electrostatic force (Hinds, 1998), as expressed in Eq. (4).

$$E_0 = F_E/q \qquad (4)$$

where F_E and q denote the electrostatic force and charge on a particle, respectively. From Eqs. (3) and (4), we can infer that an increase in surface potential can induce an increase in electrostatic force (Table S1), which
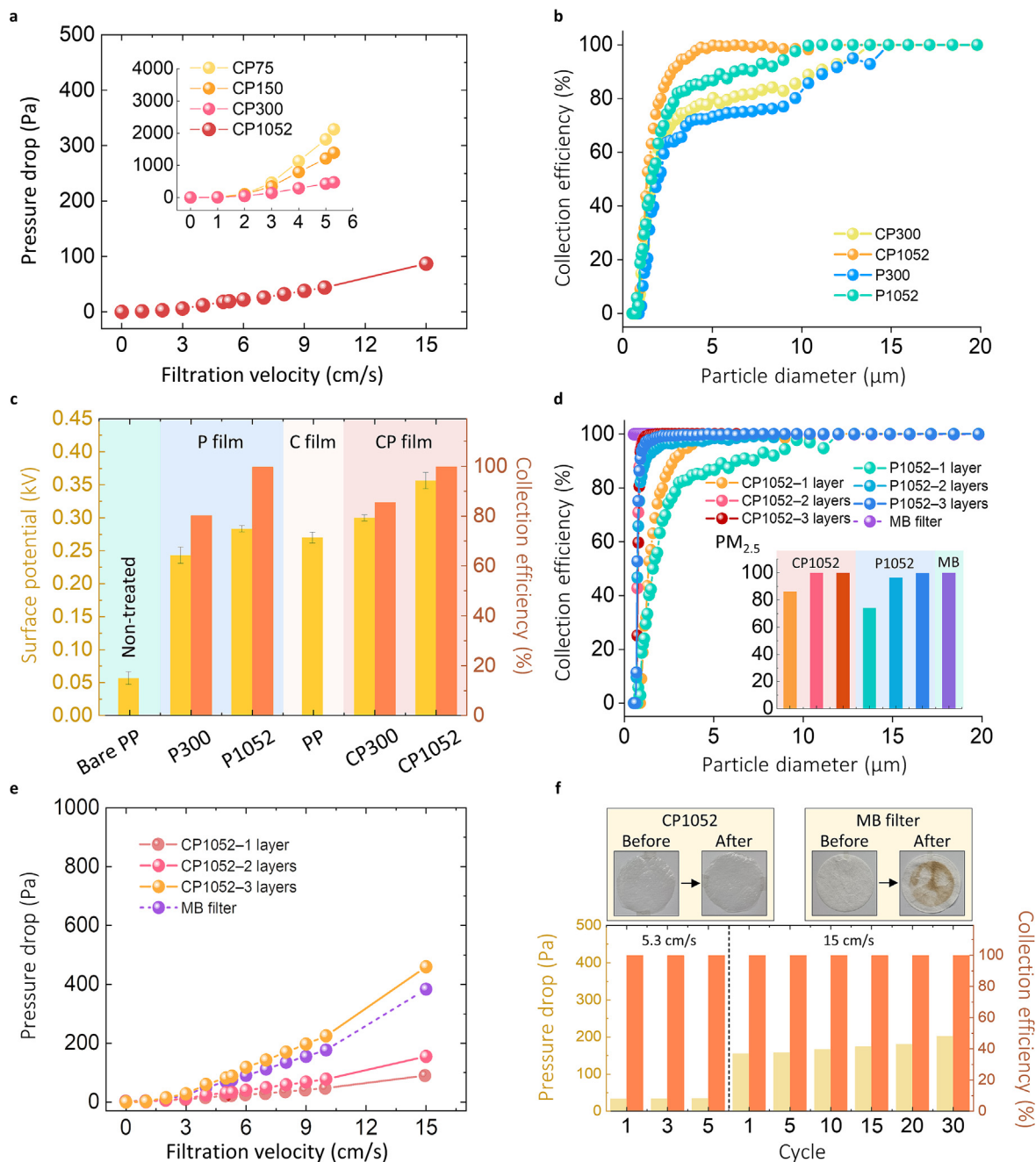
Fig. 3. Filtration capability. (a) Pressure drops of CP1052 films. Insets: Pressure drops of CP75, CP150 and CP300. (b) Collection efficiencies of fabricated filters. (c) Surface potentials and PM_{10} collection efficiencies before and after corona discharge and punching processes on transparent film. (d) Collection efficiencies of strategically stacked films with *N* of 1052. Insets: $PM_{2.5}$ collection efficiencies of samples. (e) Pressure drops of the strategically stacked CP films with *N* of 1052 and MB filter. (f) Pressure drops and collection efficiencies of CP1052 filter at the filtration velocities of 5.3 and 15 cm/s with different filtration cycles. Upper panel: Photographs showing the CP1052 (left panel) and MB filter film (right panel) before and after repeated tests at 5.3 cm/s and dusting process.

accounts for the significantly augmented collection efficiency of the CP film (Figs. 3c and 1c) (Deng et al., 2021; Lee et al., 2022). This improvement in surface potential could be explained using the following mechanisms. First, when corona discharge occurs, the applied high voltage induces ionization of the surrounding air (Tuominen et al., 2010). These ions are trapped on the PP surface, whereas the resulting free electrons penetrate deeply within the PP layer (Kravtsov and Brünig, 2000). Hence, the PP surface is charged by these trapped charge carriers, resulting in the improvement of its surface potential (Kilic et al., 2013; Kravtsov and Brünig, 2000; Popelka et al., 2018). Moreover, the surface potential could be further augmented by adjusting the corona-discharge properties such as operation time and power. For example, the enhanced corona-discharge power increases the

surface potential, which increases the surface charge density of the film (Table S1). Further improvement in surface potential can be achieved by using higher power, exceeding the 0.8 kW limit of the corona discharge apparatus used in this study. Also, we observed that the surface potentials increase and then reach saturation at ~0.27 kV with increasing duration of corona discharge (Table S1). This demonstrates that the prolonged duration of corona discharge can further enhance the surface potential, but the degree of improvement depends on the permittivity of the materials. These results are consistent with previously reported results (Das et al., 2012). Second, when two dielectric materials with distinct electrical characteristics come into contact with each other, triboelectric charging occurs owing to the electric field generated between the two materials with

different electronegativity (Kim et al., 2017; Zou et al., 2019). In our experiment, the punching process of the PP film was conducted on the PVC pad placed on a laboratory table (Table S1). We found that the surface potential generated during the punching process on the PVC pad was higher compared to the case without the PVC pad. This is attributed to the difference in electronegativity between PP and PVC (Kim et al., 2017). The interaction between the PP film and the PVC pad during the punching process results in triboelectric charging, leading to an increase in the surface potential of the PP film. In this regard, an increase in the number of punching runs leads to an increase in the surface potential of the film (Fig. 3c and Table S1), leading to improved collection efficiency of the film (Fig. 3b,c and Table S3).

To further enhance the $PM_{2.5}$ collection efficiency of the proposed microporous films, we observed the collection efficiency of strategically stacked films with $N = 1052$ (Fig. 3d). The collection efficiencies of the CP1052 and P1052 films increased as the number of stacked layers increased. Especially, the two- and three-layered stacks of CP1052 (denoted as "CP1052-2 layers" and "CP1052-3 layers") retained a collection efficiency of 99.9 % for $PM_{2.5}$, while the single-layer CP1052 film (denoted as "CP1052–1 layer") exhibited a collection efficiency of 86.0 % for $PM_{2.5}$ (Fig. 3d, inset and Table S3). After the filtration test, we observed that the particulate matter is attached over the entire surface of the filtrated CP1052 filter, while the filter is relatively clean before the test (Fig. S8a, b). This result is consistent with our suggested collection mechanism of particulate matter (Fig. 1c,d). In comparison, we observed that the pores of the MB filter are clogged by particulate matter after test (Fig. S8c,d). Similar to CP1052 filter, the stacked P films exhibited collection efficiencies of >96 % while that of the P1052–1 layer was 74.2 % (Fig. 3d, inset). However, the pressure drops of the P1052–2 layers and − 3 layers films were 1351 and 1518 Pa at the filtration velocity of 5.3 cm/s, respectively, which hindered their utilization as face masks (Fig. S7b). In comparison, the pressure drops across the two-layered and three-layered CP films was 33 Pa and 88 Pa at the filtration velocity of 5.3 cm/s, respectively (Fig. 3e). The increase in pressure drops with increasing stacked layers is attributed to the increase in thickness of our filter, ranging from 145 to 222 μm (Fig. S11). With the increase in filtration velocity, the pressure drop of two-layered CP film reached 155 Pa at a filtration velocity of 15 cm/s, which is only <0.15 % of atmospheric pressure and within the acceptable pressure drop range (Xu et al., 2016). Accordingly, the CP1052-2 layers film was considered the optimal film-based filter for face masks in terms of its filtration performance and pressure drop. Moreover, the proposed CP1052-2 layers film retained a collection efficiency of 99.9 % for $PM_{2.5}$ while its pressure drops at the filtration velocities of 5.3 cm/s were maintained after 5 filtration test cycles (Fig. 3f, lower panel). The CP1052 films maintained their intrinsic condition without residuals, whereas the commercial MB filter retained residuals after a brief dusting (Fig. 3f, upper panel). To investigate repeatability in harsh environments, we conducted additional repeat filtration tests, extending the test cycles up to 30 cycles at the filtration velocity of 15 cm/s (Fig. 3f, lower panel and Fig. S9). The increase in pressure drops of our CP1052-2 layers remained below 10 % even after 10 cycles (Fig. 3f, lower panel). After 30 cycles, we observed an inevitable increase of approximately 30 % in pressure drop, while still maintaining a high collection efficiency of over 99.9 % (Fig. 3f, lower panel). Note that despite this increase in pressure drops, our film-based filter demonstrated a relatively low performance degradation compared to a commercial MB filter. The MB filter exhibited a pressure drop increase of over 47 % after 30 cycles (Fig. S9), revealing a higher susceptibility to pore clogging compared to our suggested filter.

Furthermore, we conducted a water vapor permeability test using a custom-built apparatus as shown in Fig. S1a. We observed a gradual increase in relative humidity at CP1052-2 layers up to 55 % and reached saturation with prolonged exposure, which is analogous to a commercial MB filter (Fig. S1b). These findings indicate that our film-based filter effectively facilitates the emission of water vapor from human exhalation.

We performed a quantitative comparison of the proposed CP film with previously reported fibrous filters in terms of quality factor values, which quantifies filter performance on the basis of the relationship between filtration performance and pressure drop and they are calculated using the following equation (Fig. 4 and Table S4) (Liu et al., 2015, 2020; Niu et al., 2021; Song et al., 2020; Wang et al., 2016b; Xu et al., 2016; Yang et al., 2019; Zhao et al., 2016).

$$Quality\ factor = -\ \ln P/\Delta p\left(Pa^{-1}\right) \tag{5}$$

where P denotes the penetration of particles passing through the filter, and Δp is the pressure drop across the filter. Most previous studies were based on fiber-based approaches and achieved decent quality factors. The quality factor of the proposed CP film is higher than those of other fibrous coatings with transparency (Liu et al., 2015; Xu et al., 2016; Zhao et al., 2016), while it is comparable to those of opaque fibrous filters with a high quality factor (Wang et al., 2016b; Yang et al., 2019). More importantly, our film-based CP sample is micro-plastic free owing to the use of the film-based filter without any supporting materials. In addition, the fabrication process developed herein provides a feasible means to implement a facile and scalable transparent face mask.

3.3. Assessment of transparency and wearability

To demonstrate the applicability of the proposed CP film as a transparent face mask, we optically measured its transmittance with different numbers of stacked layers (Fig. 5a). In addition, we investigated the commercial MB filter for comparison. The measured transmittance levels of the 1- and 2-layers film filters were 72.3 and 52.0 %, respectively, at 550 nm, while the MB filter was opaque at visible wavelengths (380–780 nm (Oh et al., 2022a)). These levels of transparency allow people to perceive backgrounds, including logos, texts (Fig. 5b), and paintings (Fig. S10) through the CP film, respectively. This is because a filter with a transmittance that is higher than 50.0 % allows for clear visualization of background images (Liu et al., 2019), as evident from the camera images (Fig. 5b and Fig. S10). Especially, the faces of persons in paintings were successfully recognized by the mobile camera (Fig. S10). To support the measured results, we explored the transmittance characteristics of the prepared samples by performing finite-difference time-domain (FDTD) analysis. In Fig. S2, the top (Fig. S2a,c) and side views (Fig. S2b,d) of the geometrical models of the CP film (Fig. S2a,b) and MB filter (Fig. S2c,d) are presented. The simulation results show that the transmittance of the MB filter is almost zero in the calculated wavelength range (Fig. 5c). This is attributed to the refraction and scattering of incident light caused by the multi-layered fibrous filter structures, despite their low packing density. In comparison, in terms of
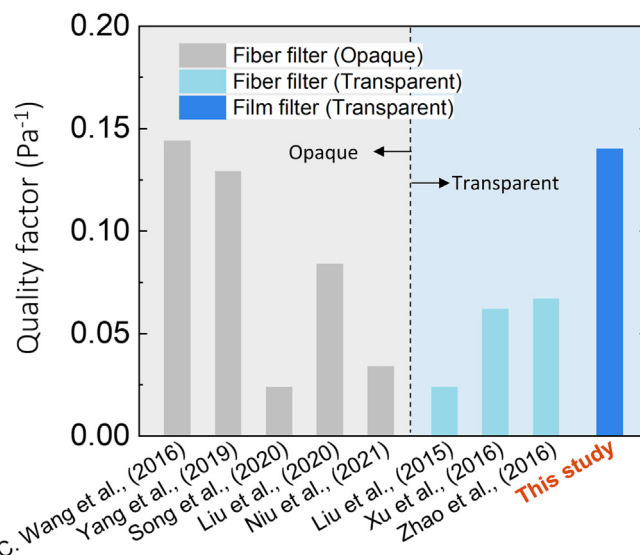

Fig. 4. Comparison of microporous film filter (CP1052-2 layers) with previously reported filters.
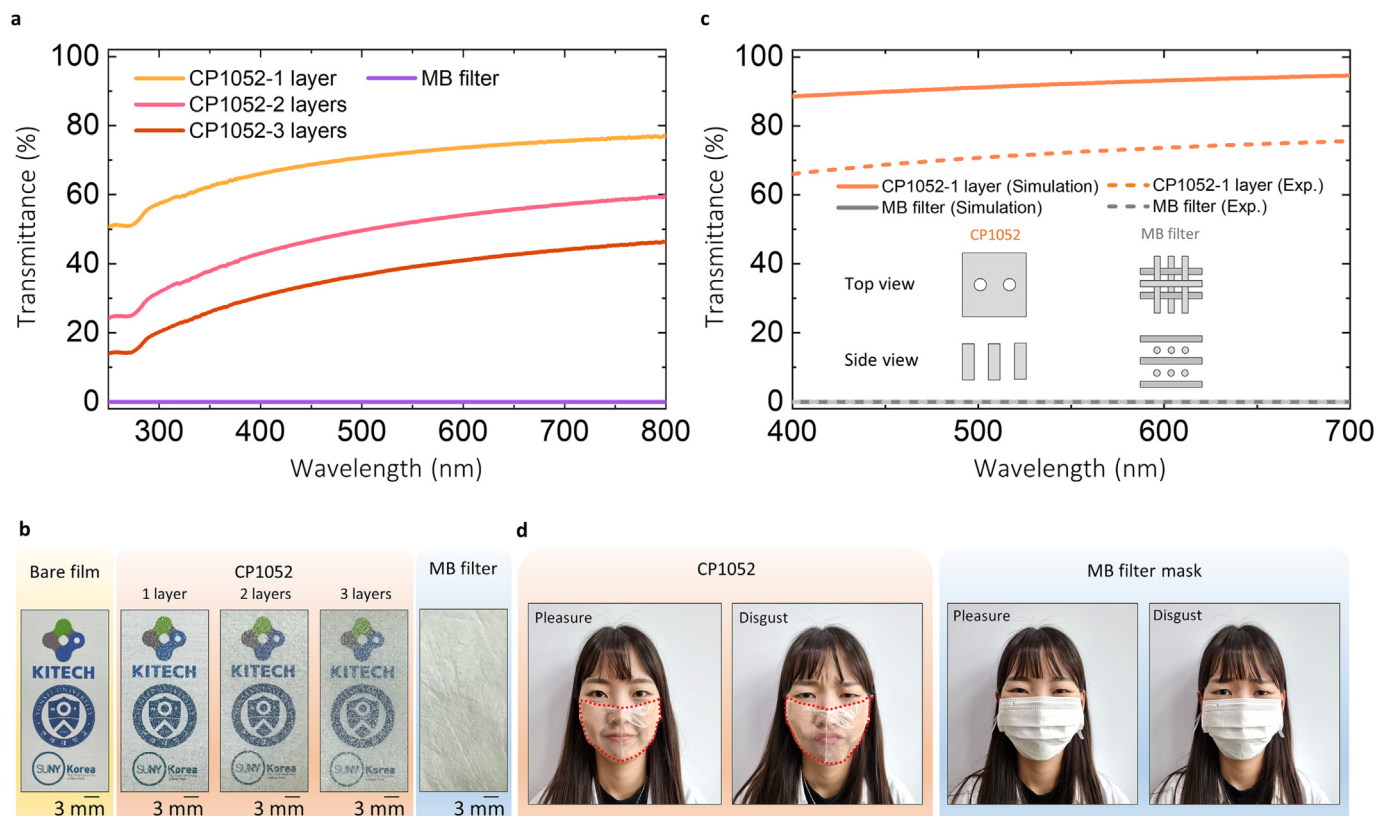
Fig. 5. Transparency assessment. (a) Transmittance of CP films with different numbers of stacked layers. (b) Transparency comparison of prepared samples. (c) Transmittance characteristics of prepared samples using finite-difference time-domain (FDTD) analysis. (d) Photographs of a person wearing a face mask made of CP1052 (left panel, red dotted lines: outlines of masks) and MB filter (right panel).

transmittance, CP1052 outperformed the MB filter, which is consistent with the measurement results (Fig. 5a). We assume that the discrepancy between the simulation and measurement results can be attributed to the roughness and internal defects of the CP film as a result of its fabrication procedure, which were not considered in the simulation.

As a proof-of-concept, we manufactured a bird's mouth-type transparent face mask composed of the proposed microporous film (Fig. 5d, left panel). We observed that the face mask provides a proper fit for a person wearing the mask. Especially, the curvature regions, including the chin and nose, are adequately covered with the improved mask (Fig. S12a–c). Note that the PP material used in our study is commonly employed in the production of commercial masks (Yu et al., 2012). Furthermore, the PP film possesses good processability, allowing it to be shaped into various shapes. Hence, we ensured that the various existing methods used in commercial masks, such as the use of elastic bands and bendable wires can also be applied to our mask to achieve proper face fitting (Fig. S12d,e). As a result, the face mask made of our film-based filter provides sufficient transparency, along with a comfortable fit, enabling the wearer's facial expressions to be perceived compared to an opaque MB filter-based face mask (Fig. 5d).

3.4. Durability of transparent microporous film

The proposed film-based filter can be frequently exposed to dust when it is utilized as a face mask. To investigate the anti-fouling capability of the proposed CP1052 film (Fig. 6a,b), we conducted a cleaning test with running water. In this experiment, water from the dispenser was made to fall onto a sample at an inclination angle (α) of 30° and a constant volume rate of 1 l/min (Fig. 6a). Fig. 6b shows laser confocal microscopy images of the CP1052 film (left panel) and MB filter (right panel) before and after the anti-fouling test, which involved contamination and cleaning. After washing with water, the CP film was restored to its pristine state

without any residual contamination surface, whereas the MB filter retained dust on its fibers. This was attributed to the fact that the CP1052 sample was a film-based filter without nanofibers, which suppressed dust infiltration and eliminated dust through a facile cleaning process. Accordingly, we assumed that the suggested CP1052 film can be reused without increasing the pressure drop across it.

In face mask utilization, one of the most important functions is blockage of droplets. To investigate the resistance of the proposed filter against liquids, the prepared samples were exposed to a water column with hydrostatic pressure (Fig. 6c). The results indicated that water did not permeate across the CP1052 film, but they did permeate through the MB3 filter after 2 h. These results indicate that the CP1052 film filter has adequate liquid resistance against water permeation, thus confirming its ability to block droplets.

Surface peeling is another significant concern when using a face mask composed of fibers because the microplastics exfoliated from the mask surface are detrimental to people (Chen et al., 2022). To investigate the surface peeling of face masks, we subjected to tape tests, as depicted in Fig. 6e. In the case of the commercial MB filter consisting of two outer layers and one inner layer (Fig. 6e, right), we observed that a large number of nanofibers were delaminated from both inner and outer layers by the tape (Fig. 6f, lower panel). In comparison, the CP1052 film did not leave any residual matter on the tape in the peeling test because it is a film-based filter, and nanofibers are not used in its fabrication (Fig. 6f, lower panel). These results indicate that the CP1052 film is relatively free of microplastics compared to the fibrous filter.

In usage of face mask, they can be exposed to mechanical stress including multiple times of folds and wears. To demonstrate the foldability of our filter, we conducted a foldability test as shown in Fig. 6g (Jia et al., 2020). We observed that our filter can be easily folded three times and then unfolded, and creases could be clearly observed. Furthermore, even after subjecting the filter to 150 cycles of folding and unfolding, the surface
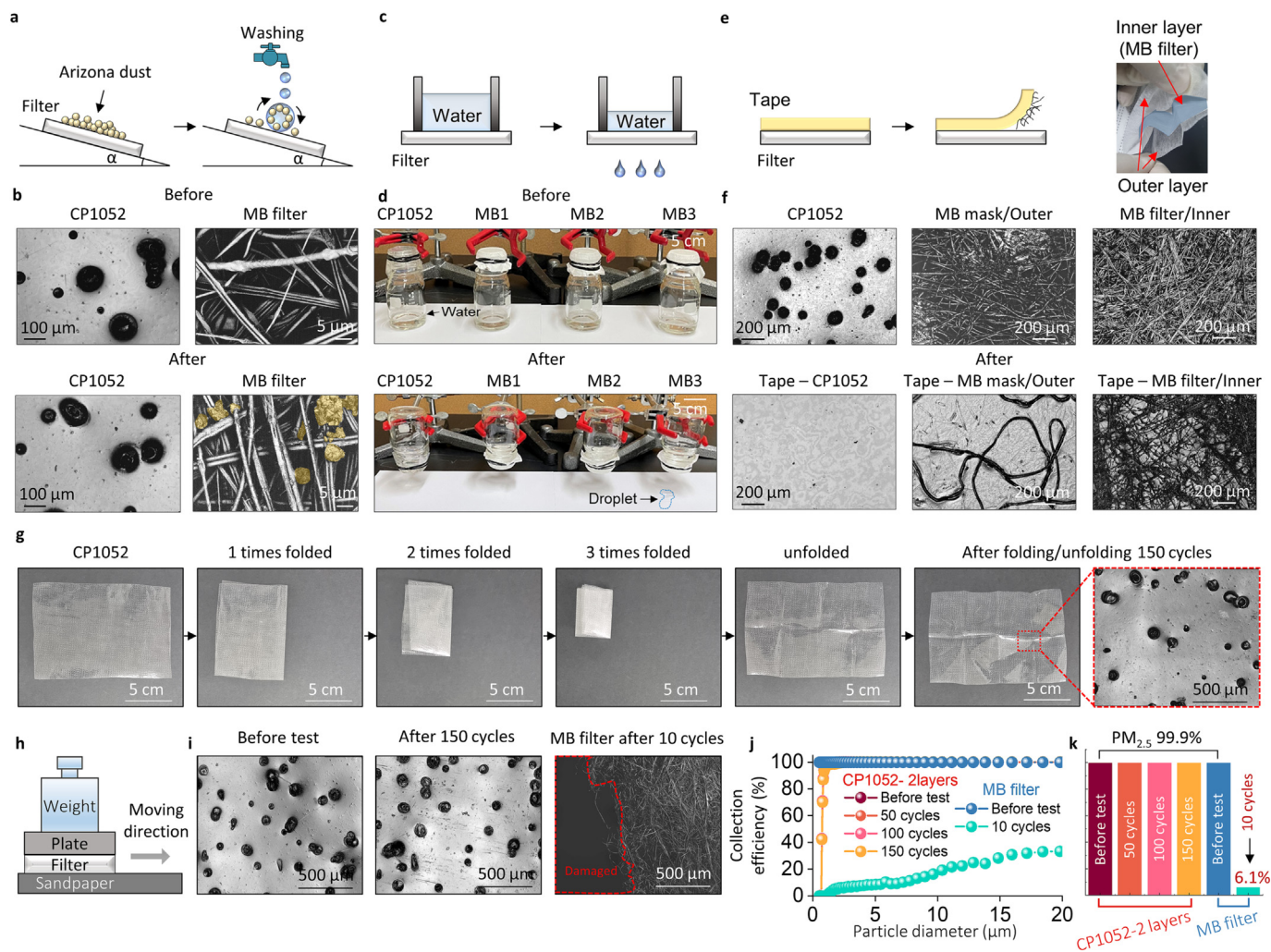
Fig. 6. Durability of proposed transparent microporous film. (a,b) Anti-fouling test; (a) schematic of test setup, and (b) laser confocal microscopy images of CP1052 and MB filter before and after the anti-fouling test. Scale bars: 100 μm (CP1052) and 5 μm (MB filter). (c,d) Liquid resistance test; (c) schematic of test setup and (d) photographs of CP 1052 and MB filter before and after the liquid resistance liquid. Scale bar: 2 cm. (e,f) Tape test; (e) schematic of tape test (left) and photographs of structures of the commercial mask (right), and (f) laser confocal microscopy images of prepared samples before the test (upper panel) and tapes after the test (lower panel). Scale bar: 100 μm. (g) Foldability of CP1052. Red dotted box: laser confocal microscopy image of folded CP 1052 after 150 cycles. (h–k) Abrasion test; (h) schematic of test setup, (i) laser confocal microscopy images of CP1052 before (left) and after (middle) test and MB filter after test, (j,k) collection efficiencies of the tested sample with different particle diameter (j), and their PM$_{2.5}$ collection efficiencies (k).

maintained its pristine morphology without any degradation (Fig. 6g, right). Also, the robustness of our filter is demonstrated from abrasion test using sandpaper (Fig. 6h). We observed that our film-based filter maintains its PM$_{2.5}$ filtration performance of 99.9 % without any surface tear after the abrasion test of 150 cycles (Fig. 6i–k and Fig. S13a). In comparison, the inner layer of the MB mask (i.e., MB filter) exhibited tearing after 10 cycles (Fig. 6i, right and Fig. S13b), which hinders the filtration of particulate matter (Fig. 6j,k). Also, we observed the formation of fluff on the surface of the outer layer of MB mask (Fig. S13c). These findings demonstrate that our filter maintains its pristine filtration capability and appearance even after mechanical stress.

4. Conclusion

In this study, we investigated a new type of transparent microporous film-based filter with a high PM$_{2.5}$ filtration performance. Scalable and facile corona-discharging and punch-stamping processes were used to fabricate the proposed transparent film-based filter. The fabricated film-based filter yielded a pressure drop of 155 Pa at 15 cm/s and a PM$_{2.5}$ collection efficiency of 99.9 %, thereby outperforming the previously reported filters.

In addition, the transparency of the proposed film-based filter allowed its use as a face mask, facilitating others to perceive the emotional expressions of people wearing the proposed film-based mask. The developed filter tolerated adverse environmental conditions, including exposures to foulants, hydrostatic pressure by water, tape peeling, folding, and abrasion and it maintained its performance without degradation and micro-plastic generation from itself. These tolerant characteristics enabled reutilization of the proposed filter after washing.

The proposed strategy for fabricating the transparent film-based filter, which involved the corona-discharge and punch-stamping processes, was highly effective. Moreover, no harmful organic solvents were used in the fabrication process. Furthermore, the proposed strategy can be applied to other plastic films such as polyethylene (PE) and polyethylene terephthalate (PET). We believe that this study will help to facilitate safe face-to-face communication between people while reducing the environmental impacts of conventional masks, and it will be possible to leverage the proposed transparent film-based filters, not only to resolve the environmental and economic issues associated with disposable PM$_{2.5}$ filters, but also to cooperate with state-of-the-art healthcare (Fu et al., 2022) and air filter systems (Mo et al., 2020).

CRediT authorship contribution statement

Woo Jin Lee: Methodology, Visualization, Investigation, Writing—Original draft.
Seungtae Oh: Investigation, Visualization, Writing—Original draft, Writing—Review and editing.
Jong-Eun Park: FDTD analysis, Investigation.
Jungho Hwang: Investigation, Writing—Original draft.
Hyeonjin Eom: Conceptualization, Investigation, Resource, Writing—Original draft, Writing—Review and editing, Supervision, Funding acquisition.
W. J. L and S. O contributed equally to this work.

Data availability

Data will be made available on request.

Declaration of competing interest

A domestic patent with application No. 10-2022-0086305 (Transparent or translucent mask with micro-sized pores; Applicant: Korea Institute of Industrial Technology; Inventors: H.E.; W.L.; S.A.) is pending. All rights to this patent are reserved by the Korea Institute of Industrial Technology. Korea Institute of Industrial Technology is a government-funded research institute in South Korea. Other authors claim no competing interests.

The authors declare the following financial interests/personal relationships which may be considered as potential competing interests:

Hyeonjin Eom reports financial support was provided by Korea Ministry of Trade Industry and Energy. Hyeonjin Eom reports financial support was provided by Korea Institute of Industrial Technology. Hyeonjin Eom has patent Transparent or translucent mask with micro-sized pores pending to Korea Institute of Industrial Technology.

Acknowledgements

Appendix A. Supplementary data

Supplementary data to this article can be found online at https://doi.org/10.1016/j.scitotenv.2023.165197.

References

Acharya, S., Rumi, S.S., Hu, Y., Abidi, N., 2021. Microfibers from synthetic textiles as a major source of microplastics in the environment: a review. Text. Res. J. 91, 2136–2156. https://doi.org/10.1177/0040517521991244.

Ahn, S., Shim, E., Kim, Y., Bae, Y.S., Eom, H., 2022. Air filtration performance enhancement of PTFE foam–coated filters at high temperatures via secondary strongly adhering PTFE nanofiber coatings. Process. Saf. Environ. Prot. 162, 914–922. https://doi.org/10.1016/j.psep.2022.04.067.

Aragaw, T.A., 2020. Surgical face masks as a potential source for microplastic pollution in the COVID-19 scenario. Mar. Pollut. Bull. 159, 111517. https://doi.org/10.1016/j.marpolbul.2020.111517.

Bian, Y., Wang, S., Zhang, L., Chen, C., 2020. Influence of fiber diameter, filter thickness, and packing density on PM2.5 removal efficiency of electrospun nanofiber air filters for indoor applications. Build. Environ. 170, 106628. https://doi.org/10.1016/j.buildenv.2019.106628.

Brugge, D., Simon, M.C., Hudda, N., Zellmer, M., Corlin, L., Cleland, S., Lu, E.Y., Rivera, S., Byrne, M., Chung, M., Durant, J.L., 2017. Lessons from in-home air filtration intervention trials to reduce urban ultrafine particle number concentrations. Build. Environ. 126, 266–275. https://doi.org/10.1016/j.buildenv.2017.10.007.

Cáceres, C.A., Mazzola, N., Frana, M., Canevarolo, S.V., 2012. Controlling in-line the energy level applied during the corona treatment. Polym. Test. 31, 505–511. https://doi.org/10.1016/j.polymertesting.2012.02.002.

Carbon, C.C., 2020. Wearing face masks strongly confuses counterparts in Reading emotions. Front. Psychol. 11, 1–8. https://doi.org/10.3389/fpsyg.2020.566886.

Chen, C., Ji, W., Zhao, B., 2019. Size-dependent efficiencies of ultrafine particle removal of various filter media. Build. Environ. 160. https://doi.org/10.1016/j.buildenv.2019.106171.

Chen, Z., Zhang, W., Yang, H., Min, K., Jiang, J., Lu, D., Huang, X., Qu, G., Liu, Q., Jiang, G., 2022. A pandemic-induced environmental dilemma of disposable masks: solutions from the perspective of the life cycle. Environ Sci Process Impacts 24, 649–674. https://doi.org/10.1039/d1em00509j.

Cui, J., Lu, T., Li, F., Wang, Y., Lei, J., Ma, W., Zou, Y., Huang, C., 2021. Flexible and transparent composite nanofibre membrane that was fabricated via a "green" electrospinning method for efficient particulate matter 2.5 capture. J. Colloid Interface Sci. 582, 506–514. https://doi.org/10.1016/j.jcis.2020.08.075.

Das, D., Thakur, R., Pradhan, A.K., 2012. Optimization of corona discharge process using box-Behnken design of experiments. J. Electrost. 70, 469–473. https://doi.org/10.1016/j.elstat.2012.07.005.

Deng, Y., Lu, T., Cui, J., Keshari Samal, S., Xiong, R., Huang, C., 2021. Bio-based electrospun nanofiber as building blocks for a novel eco-friendly air filtration membrane: a review. Sep. Purif. Technol. 277, 119623. https://doi.org/10.1016/j.seppur.2021.119623.

Desai, K., Kit, K., Li, J., Michael Davidson, P., Zivanovic, S., Meyer, H., 2009. Nanofibrous chitosan non-wovens for filtration applications. Polymer (Guildf.) 50, 3661–3669. https://doi.org/10.1016/j.polymer.2009.05.058.

Dris, R., Gasperi, J., Saad, M., Mirande, C., Tassin, B., 2016. Synthetic fibers in atmospheric fallout: a source of microplastics in the environment? Mar. Pollut. Bull. 104, 290–293. https://doi.org/10.1016/j.marpolbul.2016.01.006.

Fatihou, A., Zouzou, N., Dascalescu, L., 2017. Particle collection efficiency of polypropylene nonwoven filter media charged by triode Corona discharge. IEEE Trans. Ind. Appl. 53, 3970–3976. https://doi.org/10.1109/TIA.2017.2678979.

Fu, Q., Liu, Y., Liu, T., Mo, J., Zhang, W., Zhang, S., Luo, B., Wang, J., Qin, Y., Wang, S., Nie, S., 2022. Air-permeable cellulosic triboelectric materials for self-powered healthcare products. Nano Energy 102, 107739. https://doi.org/10.1016/j.nanoen.2022.107739.

Gitsas, A., Floudas, G., 2008. Pressure dependence of the glass transition in atactic and isotactic polypropylene. Macromolecules 41, 9423–9429. https://doi.org/10.1021/ma8014992.

Gong, J., Zhu, T., Kipen, H., Wang, G., Hu, M., Guo, Q., Ohman-Strickland, P., Lu, S.E., Wang, Y., Zhu, P., Rich, D.Q., Huang, W., Zhang, J., 2014. Comparisons of ultrafine and fine particles in their associations with biomarkers reflecting physiological pathways. Environ. Sci. Technol. 48, 5264–5273. https://doi.org/10.1021/es5006016.

Gori, M., Schiatti, L., Amadeo, M.B., 2021. Masking emotions: face masks impair how we read emotions. Front. Psychol. 12. https://doi.org/10.3389/fpsyg.2021.669432.

Grafe, T., Gragam, K., 2003. Polymeric nanofibers and nanofiber webs: a new class of nonwovens. J. Eng. Fiber. Fabr. 12, 51–55. https://doi.org/10.1177/1558925003os-120011.

Grenville, E., Dwyer, D.M., 2022. Face masks have emotion-dependent dissociable effects on accuracy and confidence in identifying facial expressions of emotion. Cogn. Res. Princ. Implic. 7. https://doi.org/10.1186/s41235-022-00366-w.

Hinds, W.C., 1998. Aerosol Technology. 2nd ed. WILEY-INTERSCIENCE.

Howard, J., Huang, A., Li, Z., Tufekci, Z., Zdimal, V., van der Westhuizen, H.M., von Delft, A., Price, A., Fridman, L., Tang, L.H., Tang, V., Watson, G.L., Bax, C.E., Shaikh, R., Questier, F., Hernandez, D., Chu, L.F., Ramirez, C.M., Rimoin, A.W., 2021. An evidence review of face masks against COVID-19. Proc. Natl. Acad. Sci. U. S. A. 118, 1–12. https://doi.org/10.1073/pnas.2014564118.

Ioannou, S.V., Raouzaiou, A.T., Tzouvaras, V.A., Mailis, T.P., Karpouzis, K.C., Kollias, S.D., 2005. Emotion recognition through facial expression analysis based on a neurofuzzy network. Neural Netw. 18, 423–435. https://doi.org/10.1016/j.neunet.2005.03.004.

Jia, C., Liu, Y., Li, L., Song, J., Wang, H., Liu, Z., Li, Z., Li, B., Fang, M., Wu, H., 2020. A foldable all-ceramic air filter paper with high efficiency and high-temperature resistance. Nano Lett. 20, 4993–5000. https://doi.org/10.1021/acs.nanolett.0c01107.

Kilic, A., Shim, E., Yeom, B.Y., Pourdeyhimi, B., 2013. Improving electret properties of PP filaments with barium titanate. J. Electrost. 71, 41–47. https://doi.org/10.1016/j.elstat.2012.11.005.

Kim, Y.J., Lee, J., Park, S., Park, C., Park, C., Choi, H.J., 2017. Effect of the relative permittivity of oxides on the performance of triboelectric nanogenerators. RSC Adv. 7, 49368–49373. https://doi.org/10.1039/c7ra07274k.

Kim, G., Seong, S.H., Hong, S.S., Choi, E., 2022. Impact of face masks and sunglasses on emotion recognition in south Koreans. PLoS One 17, 1–14. https://doi.org/10.1371/journal.pone.0263466.

Kravtsov, A.G., Brünig, H., 2000. Characteristics of electret charge formation in polyprolylene fibres. Fibre Chem. 32.

Lane, K.J., Levy, J.I., Scammell, M.K., Peters, J.L., Patton, A.P., Reisner, E., Lowe, L., Zamore, W., Durant, J.L., Brugge, D., 2016. Association of modeled long-term personal exposure to ultrafine particles with inflammatory and coagulation biomarkers. Environ. Int. 92–93, 173–182. https://doi.org/10.1016/j.envint.2016.03.013.

Lavoie, J.H., Rojas, O.J., Khan, S.A., Shim, E., 2020. Migration effects of Fluorochemical melt additives for alcohol repellency in polypropylene nonwoven materials. ACS Appl. Mater. Interfaces 12, 36787–36798. https://doi.org/10.1021/acsami.0c10144.

Lee, W.J., Kim, H. Bin, Eom, H., Hwang, J., Lee, M.-H., 2022. Effect of surface charge density on electret filters charge degradation by organic solvent exposure. Environ. Eng. Res. 28. https://doi.org/10.4491/eer.2021.523 (210523–0).

Li, H., Hou, J., Liu, X., Li, R., Zhu, H., Wu, L., 2011. Combined determination of specific surface area and surface charge properties of charged particles from a single experiment. Soil Sci. Soc. Am. J. 75, 2128–2135. https://doi.org/10.2136/sssaj2010.0301.

Liang, W., Xu, Y., Li, X., Wang, X.X., Di Zhang, H., Yu, M., Ramakrishna, S., Long, Y.Z., 2019. Transparent polyurethane nanofiber air filter for high-efficiency PM2.5 capture. Nanoscale Res. Lett. 14. https://doi.org/10.1186/s11671-019-3199-0.

Lin, Y., Li, X., Meng, L., Chen, X., Lv, F., Zhang, Q., Li, L., 2018. Stress-induced microphase separation of interlamellar amorphous phase in hard-elastic isotactic polypropylene film. Polymer (Guildf.) 148, 79–92. https://doi.org/10.1016/j.polymer.2018.06.009.

Liu, C., Hsu, P.C., Lee, H.W., Ye, M., Zheng, G., Liu, N., Li, W., Cui, Y., 2015. Transparent air filter for high-efficiency PM 2.5 capture. Nat. Commun. 6. https://doi.org/10.1038/ncomms7205.

Liu, H., Huang, J., Mao, J., Chen, Z., Chen, G., Lai, Y., 2019. Transparent Antibacterial Nanofiber Air Filters with Highly Efficient Moisture Resistance for Sustainable Particulate Matter Capture. iScience 19, 214–223. https://doi.org/10.1016/j.isci.2019.07.020.

Liu, Y., Qian, X., Wang, L., Qian, Y., Bai, H., Wang, X., 2020. Hierarchical micro/nanofibrous filter for effective fine-particle capture. Powder Technol. 360, 1192–1199. https://doi.org/10.1016/j.powtec.2019.11.012.

Lumerical FDTD Solutions, 2018. Lumerical solutions, Inc [WWW document]. https://www.lumerical.com/products/fdtd/.

Lv, D., Zhu, M., Jiang, Z., Jiang, S., Zhang, Q., Xiong, R., Huang, C., 2018. Green electrospun nanofibers and their application in air filtration. Macromol. Mater. Eng. 303, 1–18. https://doi.org/10.1002/mame.201800336.

Marler, H., Ditton, A., 2021. "I'm smiling back at you": exploring the impact of mask wearing on communication in healthcare. Int. J. Lang. Commun. Disord. 56, 205–214. https://doi.org/10.1111/1460-6984.12578.

Martinelli, N., Olivieri, O., Girelli, D., 2013. Air particulate matter and cardiovascular disease: a narrative review. Eur. J. Intern. Med. 24, 295–302. https://doi.org/10.1016/j.ejim.2013.04.001.

Martinez, J., Aghajani, M., Lu, Y., Blevins, A.K., Fan, S., Wang, M., Killgore, J.P., Perez, S.B., Patel, J., Carbrello, C., Foley, S., Sylvia, R., Long, R., Castro, R., Ding, Y., 2022. Capillary bonding of membranes by viscous polymers: infiltration kinetics and mechanical integrity of the bonded polymer/membrane structures. J. Membr. Sci. 641, 119898. https://doi.org/10.1016/j.memsci.2021.119898.

Matthews, S., Mai, L., Jeong, C.B., Lee, J.S., Zeng, E.Y., Xu, E.G., 2021. Key mechanisms of micro- and nanoplastic (MNP) toxicity across taxonomic groups. Comp. Biochem. Physiol. Part - C Toxicol. Pharmacol. 247, 109056. https://doi.org/10.1016/j.cbpc.2021.109056.

Mikheev, A.Y., Shlyapnikov, Y.M., Kanev, I.L., Avseenko, A.V., Morozov, V.N., 2016. Filtering and optical properties of free standing electrospun nanomats from nylon-4,6. Eur. Polym. J. 75, 317–328. https://doi.org/10.1016/j.eurpolymj.2016.01.001.

Miyazaki, Y., Kamatani, M., Suda, T., Wakasugi, K., Matsunaga, K., Kawahara, J.I., 2022. Effects of wearing a transparent face mask on perception of facial expressions. Iperception 13. https://doi.org/10.1177/20416695221105910 (204166952211059).

Mo, J., Zhang, C., Lu, Y., Liu, Y., Zhang, N., Wang, S., Nie, S., 2020. Radial piston triboelectric nanogenerator-enhanced cellulose fiber air filter for self-powered particulate matter removal. Nano Energy 78, 105357. https://doi.org/10.1016/j.nanoen.2020.105357.

Morgana, S., Casentini, B., Amalfitano, S., 2021. Uncovering the release of micro/nanoplastics from disposable face masks at times of COVID-19. J. Hazard. Mater. 419, 126507. https://doi.org/10.1016/j.jhazmat.2021.126507.

Nestor, M.S., Fischer, D., Arnold, D., 2020. "Masking" our emotions: botulinum toxin, facial expression, and well-being in the age of COVID-19. J. Cosmet. Dermatol. 19, 2154–2160. https://doi.org/10.1111/jocd.13569.

Niu, Z., Bian, Y., Xia, T., Zhang, L., Chen, C., 2021. An optimization approach for fabricating electrospun nanofiber air filters with minimized pressure drop for indoor PM2.5 control. Build. Environ. 188, 107449. https://doi.org/10.1016/j.buildenv.2020.107449.

Oh, S., Ki, S., Ryu, S., Shin, M.C., Lee, J., Lee, C., Nam, Y., 2019. Performance analysis of gravity-driven oil-water separation using membranes with special wettability. Langmuir 35, 7769–7782. https://doi.org/10.1021/acs.langmuir.9b00993.

Oh, S., Cho, J.W., Lee, J., Han, J., Kim, S.K., Nam, Y., 2022a. A scalable haze-free antireflective hierarchical surface with self-cleaning capability. Adv. Sci. 2202781, 1–12. https://doi.org/10.1002/advs.202202781.

Oh, S., Shim, J., Seo, D., Shim, M.J., Han, S.C., Lee, C., Nam, Y., 2022b. Organic/inorganic hybrid cerium oxide-based superhydrophobic surface with enhanced weather resistance and self-recovery. Prog. Org. Coat. 170, 106998. https://doi.org/10.1016/j.porgcoat.2022.106998.

Park, S.W., Yoo, S.H., An, S.T., Chang, S.H., 2012. Material characterization of glass/polypropylene composite bone plates according to the forming condition and performance evaluation under a simulated human body environment. Compos. Part B 43, 1101–1108. https://doi.org/10.1016/j.compositesb.2011.09.008.

Paula E Silva, E., Rosa, E.L., Barbosa, S.V., 2001. Tissue reactions of polypropylene mesh used in maxillofacial trauma. Braz. Dent. J. 12, 121–125.

Popelka, A., Khanam, P.N., Almaadeed, M.A., 2018. Surface modification of polyethylene/graphene composite using corona discharge. J. Phys. D. Appl. Phys. 51. https://doi.org/10.1088/1361-6463/aaa9d6.

Prata, J.C., da Costa, J.P., Lopes, I., Duarte, A.C., Rocha-Santos, T., 2020. Environmental exposure to microplastics: an overview on possible human health effects. Sci. Total Environ. 702, 134455. https://doi.org/10.1016/j.scitotenv.2019.134455.

Rader, B., White, L.F., Burns, M.R., Chen, J., Brilliant, J., Cohen, J., Shaman, J., Brilliant, L., Kraemer, M.U.G., Hawkins, J.B., Scarpino, S.V., Astley, C.M., Brownstein, J.S., 2021. Mask-wearing and control of SARS-CoV-2 transmission in the USA: a cross-sectional study. Lancet Digit. Heal. 3, e148–e157. https://doi.org/10.1016/S2589-7500(20)30293-4.

Rai, P.K., Lee, J., Brown, R.J.C., Kim, K.H., 2021. Environmental fate, ecotoxicity biomarkers, and potential health effects of micro- and nano-scale plastic contamination. J. Hazard. Mater. 403, 123910. https://doi.org/10.1016/j.jhazmat.2020.123910.

Reedyk, C.W., Perlman, M.M., 1968. The measurement of surface charge. J. Electrochem. Soc. 115, 49. https://doi.org/10.1149/1.2411001.

Shekaraiah, S., Suresh, K., 2021. Effect of face mask on voice production during COVID-19 pandemic: a systematic review. J. Voice https://doi.org/10.1016/j.jvoice.2021.09.027.

Shen, M., Zeng, Z., Song, B., Yi, H., Hu, T., Zhang, Y., Zeng, G., Xiao, R., 2021. Neglected microplastics pollution in global COVID-19: disposable surgical masks. Sci. Total Environ. 790, 148130. https://doi.org/10.1016/j.scitotenv.2021.148130.

Shim, J., Oh, S., Kim, S., Seo, D., Shin, S., Lee, H., Ko, Y., Nam, Y., 2023. Long-lasting ceria-based anti-frosting surfaces. Int. Commun. Heat Mass Transf. 140, 106550. https://doi.org/10.1016/j.icheatmasstransfer.2022.106550.

Shruti, V.C., Pérez-Guevara, F., Kutralam-Muniasamy, G., 2021. The current state of microplastic pollution in the world's largest gulf and its future directions. Environ. Pollut. 291. https://doi.org/10.1016/j.envpol.2021.118142.

Song, J., Gunst, U., Arlinghaus, H.F., Vancso, G.J., 2007. Flame treatment of low-density polyethylene: surface chemistry across the length scales. Appl. Surf. Sci. 253, 9489–9499. https://doi.org/10.1016/j.apsusc.2007.06.018.

Song, J., Liu, Z., Li, Z., Wu, H., 2020. Continuous production and properties of mutil-level nanofiber air filters by blow spinning. RSC Adv. 10, 19615–19620. https://doi.org/10.1039/d0ra01656j.

Strobel, M., Jones, V., Lyons, C.S., Ulsh, M., Kushner, M.J., Dorai, R., Branch, M.C., 2003. A comparison of Corona-treated and flame-treated polypropylene films. Plasmas Polym. 8, 61–95. https://doi.org/10.1023/A:1022817909276.

Tuominen, M., Lahti, J., Lavonen, J., Penttinen, T., Räsänen, J.P., Kuusipalo, J., 2010. The influence of flame, corona and atmospheric plasma treatments on surface properties and digital print quality of extrusion coated paper. J. Adhes. Sci. Technol. 24, 471–492. https://doi.org/10.1163/016942409X12561252292224.

Ueki, H., Furusawa, Y., Iwatsuki-Horimoto, K., Imai, M., Kabata, H., Nishimura, H., Kawaoka, Y., 2020. Effectiveness of face masks in preventing airborne transmission of SARS-CoV-2. mSphere 5. https://doi.org/10.1128/msphere.00637-20.

Vassiliadi, E., Tarantili, P.A., 2007. Characterization of metallized biaxially oriented polypropylene film. J. Appl. Polym. Sci. 105, 1713–1722. https://doi.org/10.1002/APP.26396.

Wang, Q., Bai, Y., Xie, J., Jiang, Q., Qiu, Y., 2016a. Synthesis and filtration properties of polyimide nanofiber membrane/carbon woven fabric sandwiched hot gas filters for removal of PM 2.5 particles. Powder Technol. 292, 54–63. https://doi.org/10.1016/j.powtec.2016.01.008.

Wang, C., Wu, S., Jian, M., Xie, J., Xu, L., Yang, X., Zheng, Q., Zhang, Y., 2016b. Silk nanofibers as high efficient and lightweight air filter. Nano Res. 9, 2590–2597. https://doi.org/10.1007/s12274-016-1145-3.

Wang, X., Xiang, H., Song, C., Zhu, D., Sui, J., Liu, Q., Long, Y., 2020. Highly efficient transparent air filter prepared by collecting-electrode-free bipolar electrospinning apparatus. J. Hazard. Mater. 385, 121535. https://doi.org/10.1016/j.jhazmat.2019.121535.

World Health Organization, 2020. Rational Use of Personal Protective Equipment (PPE) for Coronavirus Disease (COVID-19): Interim Guidance [WWW Document].

Xu, J., Liu, C., Hsu, P.C., Liu, K., Zhang, R., Liu, Y., Cui, Y., 2016. Roll-to-roll transfer of electrospun nanofiber film for high-efficiency transparent air filter. Nano Lett. 16, 1270–1275. https://doi.org/10.1021/acs.nanolett.5b04596.

Yang, Y., Boom, R., Irion, B., van Heerden, D.J., Kuiper, P., de Wit, H., 2012. Recycling of composite materials. Chem. Eng. Process. Process Intensif. 51, 53–68. https://doi.org/10.1016/j.cep.2011.09.007.

Yang, X., Pu, Y., Li, S., Liu, X., Wang, Z., Yuan, D., Ning, X., 2019. Electrospun polymer composite membrane with superior thermal stability and excellent chemical resistance for high-efficiency PM2.5 capture. ACS Appl. Mater. Interfaces 11, 43188–43199. https://doi.org/10.1021/acsami.9b15219.

Yovcheva, T.A., Avramova, I.A., Mekishev, G.A., Marinova, T.S., 2007. Corona-charged polypropylene electrets analyzed by XPS. J. Electrost. 65, 667–671. https://doi.org/10.1016/j.elstat.2007.05.002.

Yovcheva, T., Babeva, T., Nikolova, K., Mekishev, G., 2008. Refractive index of corona-treated polypropylene films. J. Opt. A Pure Appl. Opt. 10. https://doi.org/10.1088/1464-4258/10/5/055008.

Yu, B., Han, J., He, X., Xu, G., Ding, X., 2012. Effects of tourmaline particles on structure and properties of polypropylene filtration melt-blown nonwoven electrets. J. Macromol. Sci. Part B Phys. 51, 619–629. https://doi.org/10.1080/00222348.2011.598098.

Yuan, X., Chung, T.C.M., 2011. Cross-linking effect on dielectric properties of polypropylene thin films and applications in electric energy storage. Appl. Phys. Lett. 98, 1–4. https://doi.org/10.1063/1.3552710.

Zhang, H., Liu, J., Zhang, X., Huang, C., Jin, X., 2018. Design of electret polypropylene melt blown air filtration material containing nucleating agent for effective PM2.5 capture. RSC Adv. 8, 7932–7941. https://doi.org/10.1039/c7ra10916d.

Zhang, D., Cui, Y., Zhou, H., Jin, C., Yu, X., Xu, Y., Li, Y., Zhang, C., 2020. Microplastic pollution in water, sediment, and fish from artificial reefs around the Ma'an Archipelago, Shengsi, China. Sci. Total Environ. 703, 134768. https://doi.org/10.1016/j.scitotenv.2019.134768.

Zhao, X., Wang, S., Yin, X., Yu, J., Ding, B., 2016. Slip-effect functional air filter for efficient purification of PM 2.5. Sci. Rep. 6, 1–11. https://doi.org/10.1038/srep35472.

Zou, H., Zhang, Y., Guo, L., Wang, P., He, X., Dai, G., Zheng, H., Chen, C., Wang, A.C., Xu, C., Wang, Z.L., 2019. Quantifying the triboelectric series. Nat. Commun. 10, 1–9. https://doi.org/10.1038/s41467-019-09461-x.